Supporting Information: Softened Elastic Response and Unzipping in CVD Graphene Membranes

Carlos S. Ruiz-Vargas[1]*, Houlong L. Zhuang*[2]*, Pinshane Y. Huang*[1]*,*

Arend M. van der Zande[3]*, Shivank Garg*[4]*, Paul L. McEuen*[3,5]*, David A. Muller*[1,5]*,*

Richard G. Hennig[2] *and Jiwoong Park*[4,5]***

1. School of Applied and Engineering Physics, Cornell University, Ithaca, NY 14853

2. Department of Material Science and Engineering, Cornell University, Ithaca, NY 14853

3. Department of Physics, Cornell University, Ithaca, NY 14853

4. Department of Chemistry and Chemical Biology, Cornell University, Ithaca, NY 14853

5. Kavli Institute at Cornell for Nanoscale Science, Cornell University, Ithaca, NY 14853

* Corresponding Author: jpark@cornell.edu

Supporting Information Contents

1. Graphene Growth and Sample Fabrication:

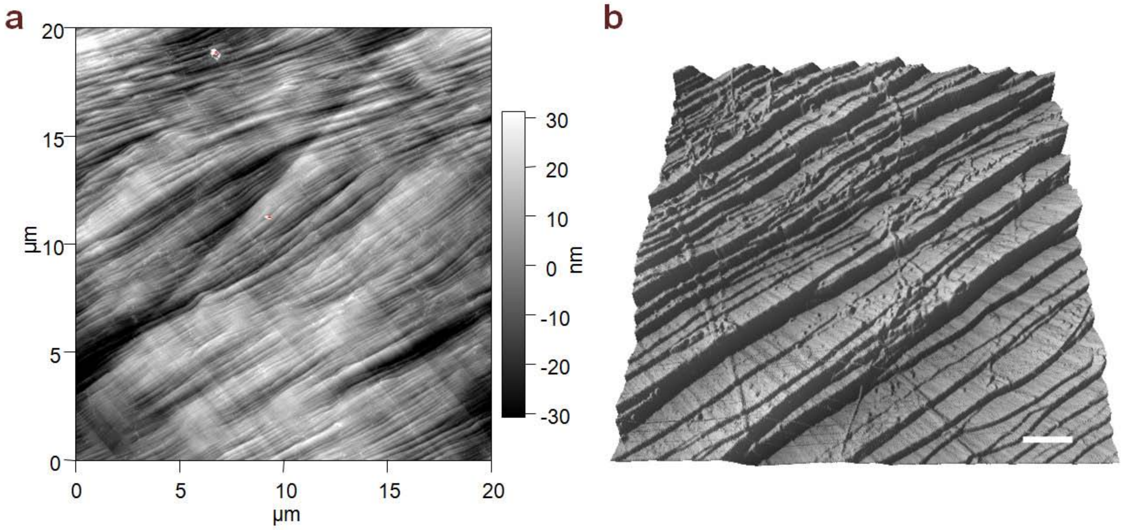

Figure S1. AFM images of a copper substrate after graphene growth. a) Region 20 microns in size b) 3D image from a zoomed in region. Scale bar: 500 nm.

Single-layer CVD graphene was grown using a similar process previously reported in the literature[1], utilizing copper foil (Alfa Aesar #13382) as the growth substrate. Growth was done at 1000° C for 10 minutes in low pressure (~10 torr), with a flow of CH_4:H_2 (875:300 scmm). AFM images of the copper surface after graphene growth are show in Fig. S1. We confirmed with Raman spectroscopy that the resulting films were predominantly single layer graphene (SLG).[2]

CVD graphene films are then transferred onto the target substrate in order to form suspended membranes. We utilized a very thin protective polymer layer (PMMA) for the transfer, followed by a liquid-free removal of the polymer (baking in hot air), which results in much higher yields (see below for a detailed recipe). Our target substrates were pre-patterned nitride grids (Fig. 1a, main manuscript). These were fabricated on Si wafers coated with LPCVD low-stress silicon nitride using standard photolithography and reactive ion etching, followed by an anisotropic KOH etch to expose the silicon nitride layer from the backside.

We found that using very thin protective PMMA layers (< 100nm) is important, since it promotes conformal adhesion of graphene to receiving substrate. Thicker PMMA layers impede this by stiffening the PMMA/graphene film, resulting in extensive tearing in the graphene membranes when the polymer is removed. Once the sample is dry, the samples are baked for 3-4 hours at 300-350° C. PMMA decomposes at these temperatures[3] allowing for a gentler dry release of the graphene membrane from its protective polymer support. We found that baking our samples directly in air resulted in a cleaner and much faster PMMA removal than under an Ar flow. This fabrication method produces suspended graphene membranes with a high yield exceeding 90% for grids containing more than 10,000 2 µm holes. We were also able to fabricate suspended graphene sheets as large as 30 µm, which were the largest dimensions we attempted to fabricate.

2. Air Chambers Sealed by CVD Graphene:

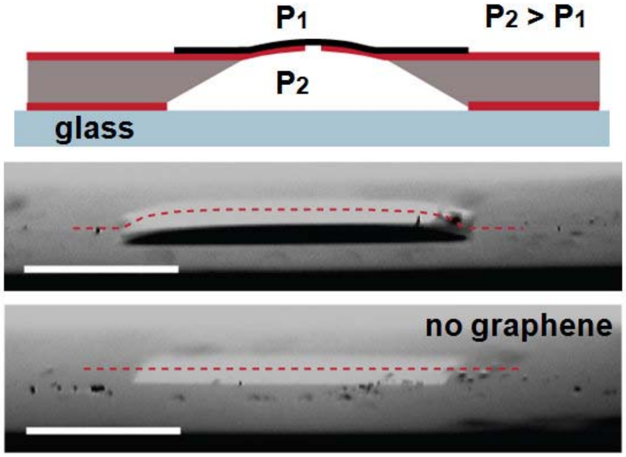

Figure S2. a) Optical side view of a chamber capped with a silicon nitride membrane with a single 3 µm hole (not visible at this magnification), with and without graphene. The nitride membrane which is covered with graphene experiences bulging due to a difference in pressure across this sealed nitride membrane. Scale bar: 1 mm.

We confirmed that our CVD graphene membranes can seal large chambers (volume ~ 2 µl) for up to 72 hours. This experiment was carried out by sealing the backside of a chip using a glass slide with vacuum grease forming an isolated air chamber. We estimate a pressure difference across the graphene sheet, caused by pressing the glass slide against the device, to be around 5000 Pa, as estimated by measuring the deflection of the nitride membrane.[4]

3. Fabrication of Double Layer Graphene Membranes:

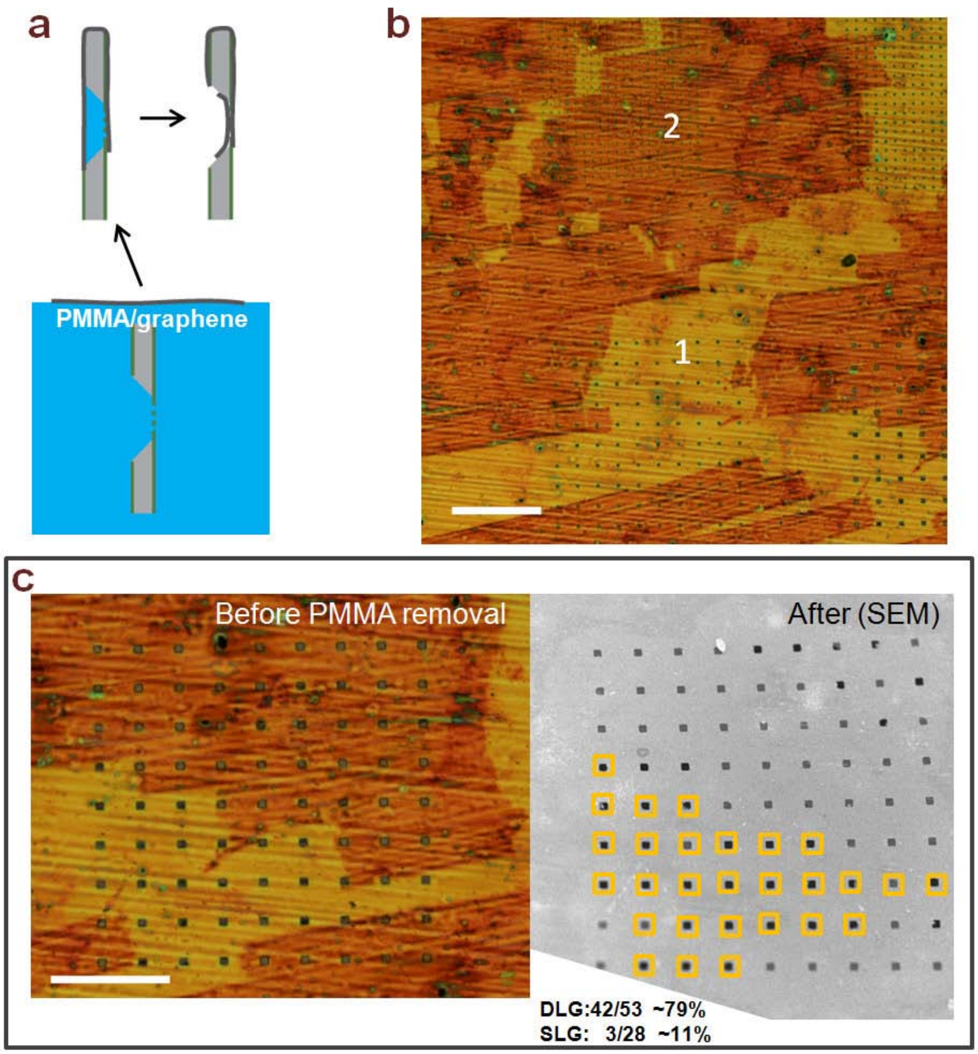

Figure S3. a) Schematic of double layer graphene (DLG) fabrication by scooping a PMMA/graphene film vertically, thus transferring it to both sides of a holey nitride membrane. b) Optical image of a nitride membrane after PMMA/graphene transfer. Darker regions (marked 2) have such a layer successfully transferred to both front and back of the nitride membrane. Scale bar: 200 µm. c) Optical image of a nitride membrane with dark regions corresponding to a PMMA/graphene layer on both sides of the nitride membrane. The holes are 10 by 10 µm. b) Scanning electron micrograph of the same region, after PMMA is removed by thermal decomposition. Yield in regions with a double layer is significantly higher (~79%) in comparison with the regions with only a single layer (~11%).

For double layer graphene (DLG) samples, a similar fabrication process was followed, with a modification in the way PMMA/graphene films were scooped onto the target substrates as shown in the schematic shown in Fig. S2a. Transferring graphene both sides of the nitride grids results in double layer graphene over the holes after the removal of PMMA (PMMA is still present in Fig. S3b). The yield is noticeably higher for the membranes where PMMA covers both sides of the nitride grid (darker regions), as can be seen in the SEM image in Fig. S3c.

4. AFM Imaging and Nanoindentation Measurements:

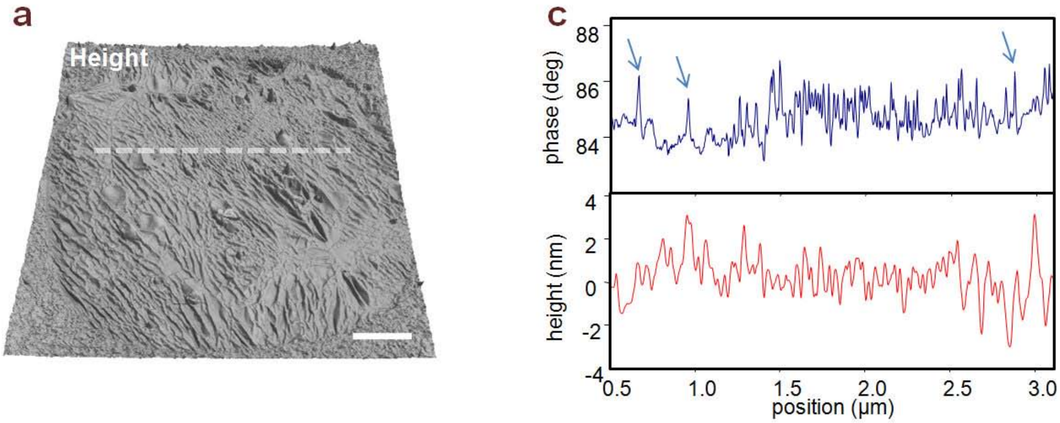

Figure S4. a) AFM height image as shown in the main manuscript. b) Phase and height traces taken along the dashed line in a, the locations of visible grain boundaries are denoted in the phase trace by the arrows.

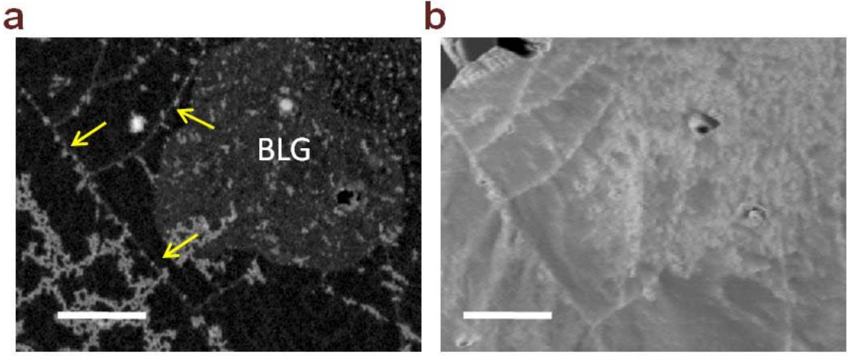

Figure S5. a) STEM image of single layer graphene, and a bilayer graphene visible as marked in the image. The arrows show the location of grain boundaries visible in graphene as it has been confirmed by the diffraction pattern obtained across these features. b) AFM phase image of the same region, with the grain boundaries visible. The bilayer graphene region is also discernable. Scale bars: 200 nm.

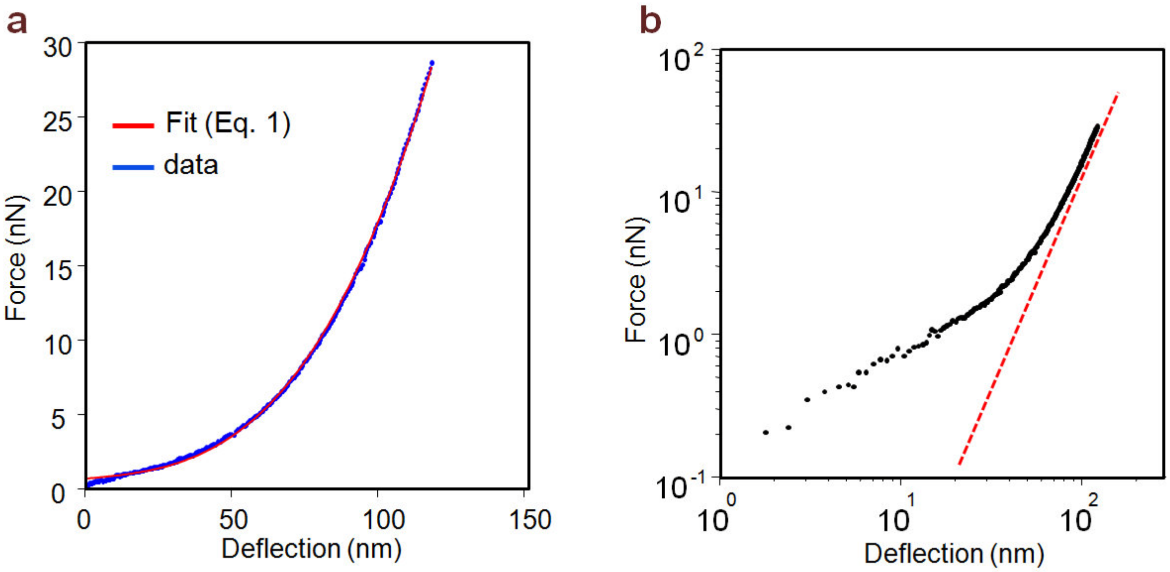

Figure S6. a) Force curve showing both the data and the model used to calculate the 2D elastic modulus, a good fit can be seen. b) Same data plotted on a log-log scale, shown approaching cubic behavior (dashed line).

We employed atomic force microscopy (AFM) to image suspended graphene sheets (Fig S2). We used a MFP-3D model, by Asylum Research and cantilevers with resonant frequencies ~75 KHz and force constant of ~3 N/m (Multi75Al, Budget Sensors). All AFM images were taken in tapping mode.

We were able to identify graphene's grain boundaries in the phase mode, as shown in Fig. S5 as well as previously reported[5]. Based on this mapping of grain boundaries, indentation points were selected, and force curves were obtained there. Following a model similar to the one described by Lee *et al.*,[6] we have calculated values of 2D elastic Young's modulus for our membranes as well as existing pretension, by fitting our data to the following expression: $F = 2\pi\sigma d / \ln\frac{a}{r} + E\,(qd)^{3}/a^{2}$. Here, σ and *E* are the 2D pretension and 2D effective Young's modulus, respectively. The parameters, *d*, a, and *r*, are the vertical deflection, the membrane's radius and the radius of the AFM tip, respectively. [7, 8] Finally, q (which is roughly 1.02)[6] is a function of the Poisson's ratio. We note that the shape of our membranes is square with rounded corners, and we assume our membranes to be circular, with a radius of 1.75 µm resulting in an uncertainty in our calculation of ~ 5%. This model provides a close fit to our data, as seen in Fig. S6a. The data approaches cubic behavior (dashed line, Fig. S6b) for large deflections, the regime from which the effective 2D elastic modulus is calculated.

The average values for the pretension extracted from the linear term of the model is σ ~ 0.085 N/m. This value predicts a lower mode of the resonant frequency for these membranes to be ~15-50 MHz, in good agreement with recent experimental results.[9] This is calculated by using the following expression: $= \frac{1}{4a}(\sigma/\rho_o\alpha)^{1/2}$. Here, a is the radius of the membrane and α, the ratio of adsorbed mass, assumes typical values[9] in the range of 1 to 10. For this calculation we used the density of single layer graphene, ρ_o , which is 7.4 x 10^{-7} kg/m^2.

5. Molecular Dynamics Simulations:

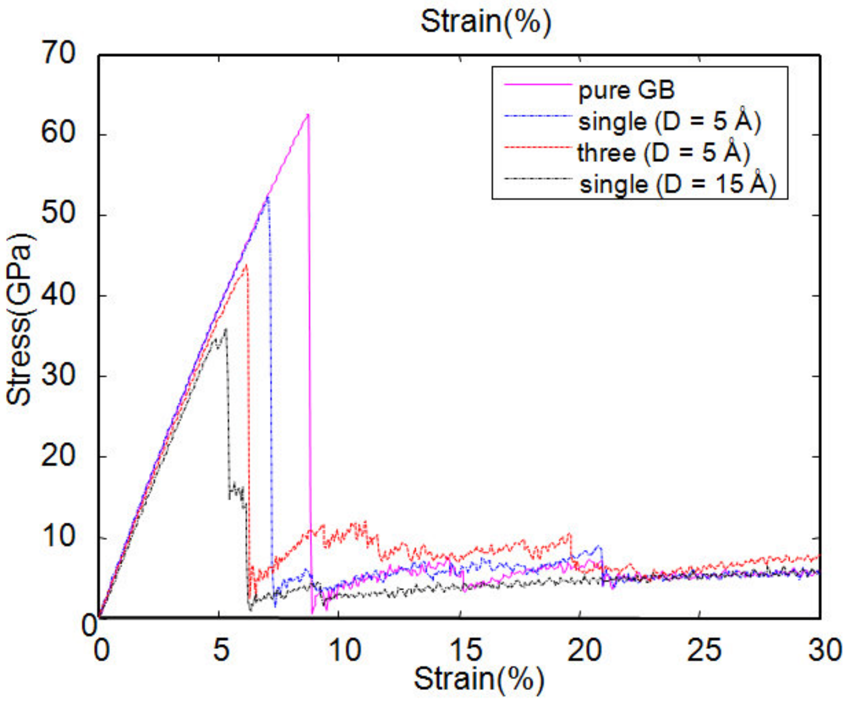

Figure S7. MD simulations of the effect of a void at the grain boundary with diameter *D*, as well as the case of multiple voids.

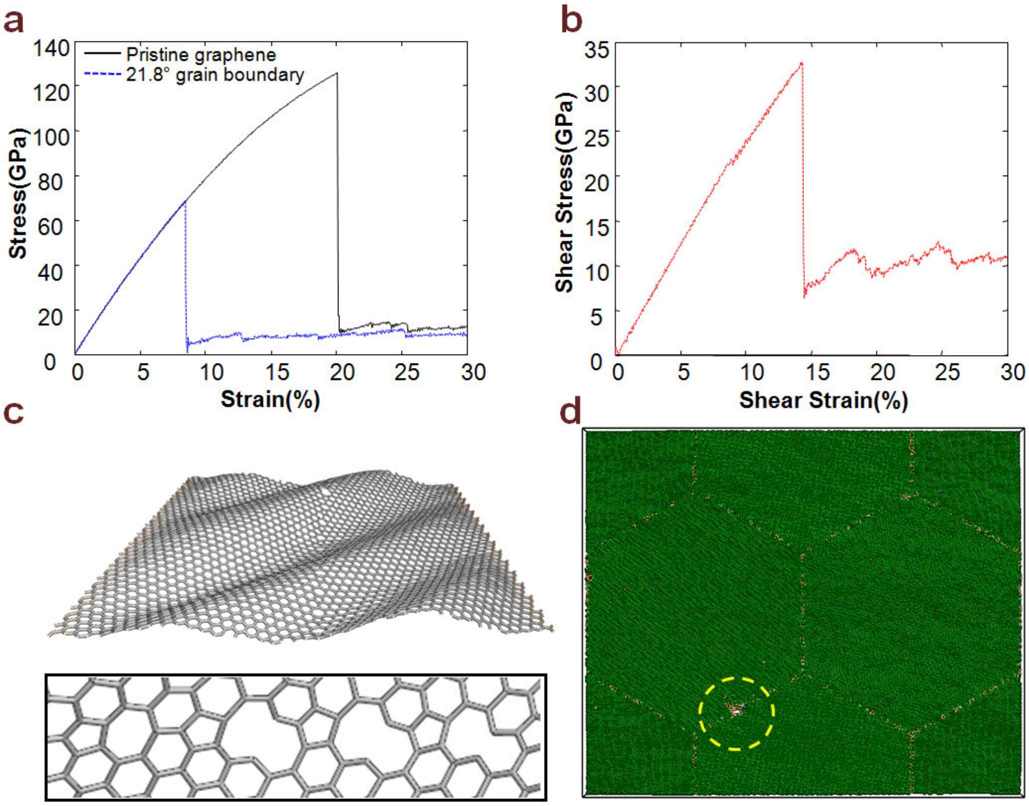

Figure S8. a) Stress-strain curves for pristine graphene and graphene with a 21.8° grain boundary. The maximum stresses are 126 GPa and 69 GPa, respectively, which agree well with previously reported values found in the literature.[13, 14] b) Shear stress-strain curve for graphene with a grain boundary. The maximum shear stress of 32 GPa is comparable to the coupling effect of grain boundary and void as discussed in the context. c) Snapshot of pure shear loading at critical strain and zoomed-in region of the grain boundary. Interestingly, the C-C bond in 7-membered rings always break first. d) Polycrystalline graphene model containing four grains with random misorientation angles. Atoms are color coded by coordination number. The region enclosed by the yellow dashed line demonstrates that the fracture starts from the grain boundary that is not normal to the tensile direction.

We performed molecular dynamics (MD) simulations of the mechanical response of graphene to tensile load using the second generation reactive empirical bond order (REBO) potential[10] in the LAMMPS program.[11] The REBO potential has been widely applied to various carbon based nanomaterials. To avoid the well-known cutoff problem for bond breaking[12] in the REBO potential, we used the modified cutoff value (2.0Å) of the covalent interaction which minimizes the spurious overestimate of the interatomic forces. Simulations are performed at 300 K with a strain rate of 0.0005/picosecond and an integration timestep of 1fs. Before loading the graphene, we equilibrated the different systems for 40 picoseconds in the NPT ensemble at room temperature to minimize the stresses. Then we applied the engineering strains and monitored the atomic stress tensor. The interlayer distance in graphite (3.4Å) is employed as the graphene thickness in calculating the total stresses. We validated our approach using the stress-strain curves for perfect graphene and graphene with pure grain boundaries. Our results for the stress-strain curves (Fig. S8a) are consistent with other reports either from simulations[13, 14] or experiment.[6]

The simulated geometry of bicrystalline graphene was based on a dislocation model[15] for small-angle grain boundaries, where the grain boundary consists of a chain of 5-7 membered carbon rings. Depending on the grain boundary angle, the distance between pairs of 5-7 membered rings varies. In this paper, we focused on one specific grain boundary with an angle of 21.8° for which the pairs of 5-7 membered rings are next to each other (see Fig. 4c). We studied how the presence of voids affects the tensile and shear strength of this boundary. Our calculations show that the presence of voids with a diameter of 5 Å in the boundary (see Fig. 4c) reduces the shear strength from 32 GPa to 25 GPa. This 22% reduction of the shear strength is slightly larger than the 15% reduction observed for the tensile strength.

REFERENCES

1. Li, X.; Cai, W.; An, J.; Kim, S.; Nah, J.; Yang, D.; Piner, R.; Velamakanni, A.; Jung, I.; Tutuc, E.; Banerjee, S. K.; Colombo, L.; Ruoff, R. S. *Science* **2009**, *324,* 1312-1314.

2. Ferrari, A. C. *Phys. Rev. Lett.* **2006**, *97,* 187401.

3. Jiao, L.; Fan, B.; Xian, X.; Wu, Z.; Zhang, J.; Liu, Z. *J. Am. Chem. Soc.* **2008**, *130,* 12612-12613.

4. Karimi, A.; Shojaei, O. R.; Kruml, T.; Martin, J. L. *Thin Solid Films* **1997**, *308-309,* 334-339.

5. Huang, P. Y.; Ruiz-Vargas, C.; v.d. Zande, A.; Whitney, W. S.; Levendorf, M. P.; Kevek, J. W.; Garg, S.; Alden, J. S.; Hustedt, C. J.; Zhu, Y.; Park, J.; McEuen, P. L.; Muller, D. A. *Nature* **2011**, *469,* 389-392.

6. Lee, C.; Wei, X.; Kysar, J. W.; Hone, J. *Science* **2008**, *321,* 385-388.

7. Wan, K.; Guo, S.; Dillard, D. A. *Thin Solid Films* **2003**, *425,* 150-162.

8. Bunch, J. S.; Verbridge, S. S.; Alden, J. S.; v.d. Zande, A.; Parpia, J. M.; Craighead, H. G.; McEuen, P. L. *Nano Lett.* **2008**, *8 (8),* 2458-2462.

9. van der Zande, A.; Barton, R. A.; Alden, J. S.; Ruiz-Vargas, C.; Whitney, W. S.; Pham, P. H. Q.; Park, J.; Parpia, J. M.; Craighead, H. G.; McEuen, P. L. *Nano Lett.* **2010**, *10 (12),* 4869-4873.

10. Stuart, S. J.; Tutein, A. B.; Harrison, J. A. *J. Chem. Phys.* **2000**, *112,* 6472-6486.

11. Plimpton, S. *Journal of Computational Physics* **1995**, *117,* 1-19.

12. Belytschko, T.; Xiao, S. P.; Schatz, G. C.; Ruoff, R. S. *Phys.Rev.B* **2002**, *65,* 235430.

13. Grantab, R.; Shenoy, V. B.; Ruoff, R. S. *Science* **2010**, *330,* 946-948.

14. Pei, Q. X.; Zhang, Y. -.; Shenoy, V. B. *Nanotechnology* **2010,** *21*, 115709.

15. Yazyev, O. V.; Louie, S. G. *Phys. Rev. B* **2010**, *81,* 195420.